Correspondence to:

K. Hättig,
katrin.haettig@nioz.nl

Stable Middle Miocene Seawater Isotopes in the Eastern North Atlantic Ocean

Katrin Hättig[1] [ORCID], **Stefan Schouten[1,2], Stephen Louwye[3]** [ORCID], **and Marcel van der Meer[1]** [ORCID]

[1]Department of Marine Microbiology and Biogeochemistry, NIOZ Royal Netherlands Institute for Sea Research, Den Burg, The Netherlands, [2]Department of Earth Sciences, Utrecht University, Utrecht, The Netherlands, [3]Department of Geology, Ghent University, Ghent, Belgium

Abstract The Middle Miocene is characterized by a long-term increase in the stable oxygen isotopic composition of benthic foraminifera ($\delta^{18}O_{benthic}$). However, it is unclear to what extent this increase reflects changes in seawater isotopic composition or deep water temperature. We present a high-resolution alkenone hydrogen isotope (δ^2H_{C37}) record of the Middle Miocene from a core taken at the upper slope edge (about 409 m water depth) of the Porcupine Basin continental margin in the eastern North Atlantic Ocean, Site U1318 of the Integrated Ocean Drilling Program. The δ^2H_{C37} values vary between −174 and −200‰ with an average of −191 ± 5‰, similar to modern open-ocean values. Importantly, they do not show a long-term increase in surface seawater isotopes (δ^2H_{SSW}) during the Middle Miocene Climate Transition. Indeed, when $\delta^{18}O_{benthic}$ is corrected for subsurface temperature, the bottom seawater oxygen isotopes ($\delta^{18}O_{BSW}$) show no significant increase in this period. When the latter record is translated into the hydrogen isotopic composition of bottom seawater using the modern open-ocean waterline, it has an average value of 5.8 ± 1.5‰, similar to the δ^2H_{SSW} of 5.2 ± 3.1‰ derived from $\delta^2H_{C37:2}$, suggesting a relatively small difference between bottom and surface waters. Our results suggest a stable global surface seawater isotope evolution during the Middle Miocene, coupled with a long-term decrease in bottom water temperature.

1. Introduction

The Miocene epoch (23.03–5.33 million years; Cohen et al., 2013) is a globally warm period compared to present day, with CO_2 concentrations varying from pre-industrial to two times higher than at present (Goldner et al., 2014). Most prominent are the Middle Miocene Climate Optimum (MMCO; 16.9–14.7 Ma) and Middle Miocene Climate Transition (MMCT; 14.7–13.8 Ma) where geological, faunal and floral evidence suggest an Antarctic ice sheet retreat and expansion, respectively (e.g., Fielding et al., 2011; Hauptvogel & Passchier, 2012; Levy et al., 2016; Passchier et al., 2011; Pierce et al., 2017; Sangiorgi et al., 2018; Warny et al., 2009). These periods are associated with changes in CO_2 concentrations (Badger et al., 2013; Greenop et al., 2014; Kürschner et al., 2008; Sosdian et al., 2018; Super et al., 2018; Zhang et al., 2013) and characterized by long-term changes in the benthic foraminifera oxygen isotopes ($\delta^{18}O_{benthic}$) (Cramer et al., 2009; Mudelsee et al., 2014; Zachos et al., 2008). Furthermore, the period is also characterized by so-called Miocene oxygen isotope excursions events (Mi-events) (Miller et al., 1991), globally observed short-lived (ca. 100 kyrs) changes in $\delta^{18}O_{benthic}$ (Cramer et al., 2009; Mudelsee et al., 2014), likely representing a decrease in deep-water temperature and/or seawater isotopic composition changes caused by cryosphere expansion and associated with sea-level variations of tens of meters (John et al., 2011; Levy et al., 2019; Miller et al., 2020; Shevenell et al., 2004, 2008). However, our understanding of ice volume estimates and long-term climate change during this period largely builds on the oxygen isotopic composition of benthic foraminifera (Miller et al., 2020; Westerhold et al., 2020) a proxy which reflects not only the isotopic composition but also the temperature of seawater (e.g., Savin et al., 1975; Shackleton, 1974). Deep ocean temperature can potentially be constrained by Mg/Ca or carbonate clumped isotopes of foraminiferal shells (Billups & Schrag, 2003; Elderfield et al., 2012; Hou et al., 2023; Lear et al., 2000; Modestou et al., 2020; S. Sosdian & Rosenthal, 2009). Modestou et al. (2020) measured Mg/Ca and Δ_{47} on the same Miocene foraminifera and observed good agreement between the two temperature estimates. Their Δ_{47} temperature change of approximately 2.9°C recorded over the MMCT would result in a bottom seawater oxygen isotope ($\delta^{18}O_{BSW}$) change of ca. 0.6‰. The Δ_{47} results from Hou et al. (2023) show that Middle Miocene bottom water temperature (BWT) dropped by ca. 5°C in the Southern Ocean during the MMCT and their calculations indicate that $\delta^{18}O_{BSW}$ was constant over this time, suggesting ice volume was stable. Furthermore, absolute $\delta^{18}O_{BSW}$ values were close to the modern seawater isotopic composition despite the much warmer global climate.

Visualization: Katrin Hättig,
Stefan Schouten, Marcel van der Meer
Writing – original draft: Katrin Hättig
Writing – review & editing:
Stefan Schouten, Stephen Louwye,
Marcel van der Meer

This contrasts with earlier estimates of a smaller temperature change during the MMCT and therefore a clear increase in $\delta^{18}O_{SW}$ and ice volume (e.g., Billups & Schrag, 2003; Lear et al., 2000, 2015; Shevenell et al., 2008). Thus, it is not entirely clear how the seawater isotopic compositions evolved over the Middle Miocene due to the different corrections and temperature proxies used to reconstruct bottom water oxygen isotope records from $\delta^{18}O$ benthic foraminiferal records.

Another potential proxy for the isotopic composition of seawater is based on the hydrogen isotopic composition of long chain alkenones (δ^2H_{C37}), produced by haptophyte algae. Culture studies show that hydrogen isotopic fractionation of phototrophic organisms depends on, amongst others, the hydrogen isotopic composition of growth water and salinity (M'Boule et al., 2014; Sachs et al., 2016; Schouten et al., 2006; Weiss et al., 2017; Zhang et al., 2009; Zhang & Sachs, 2007). Gould et al. (2019), based on open-ocean suspended particulate organic matter (SPOM), and Mitsunaga et al. (2022), based on core top sediments, show a statistically identical relationship between δ^2H_{C37} and the hydrogen isotopic composition of surface water (δ^2H_{SSW}). This suggests that in the natural environment, the influence of factors such as temperature, salinity, species composition (e.g., Chivall et al., 2014; M'Boule et al., 2014), as well as light and nutrient availability (Sachs et al., 2017; van der Meer et al., 2015) on stable hydrogen isotope fractionation during biosynthesis might be less important than the hydrogen isotopic composition of seawater. Hättig et al. (2023) used these calibrations to reconstruct δ^2H_{SSW} for the last glacial maximum and found that δ^2H ratios of alkenones are a reproducible paleo-proxy for relative changes in seawater hydrogen isotope composition and that alkenone δ^2H values fit with other isotope records. Therefore, the hydrogen isotopic composition of alkenones has the potential to produce hydrogen isotope records of surface seawater, independent of temperature.

Here we present a hydrogen isotope record of the $C_{37:2}$ alkenone ($\delta^2H_{C37:2}$) spanning most of the Middle Miocene from 16.60 Ma till 12.75 Ma from a shelf site (Site U1318, ~400 m water depth) in the Porcupine Basin, in the eastern North Atlantic, and compare it to the local benthic foraminiferal $\delta^{18}O$ record previously published by Quaijtaal et al. (2018). The latter record showed the clear impact of the MMCT by a substantial increase in benthic $\delta^{18}O$ values of 1‰ in line with the global benthic stack (Westerhold et al., 2020). Furthermore, the Porcupine Basin foraminiferal stable isotope record shows imprints of some Mi-events (Quaijtaal et al., 2018). We reconstructed the oxygen isotopic composition of bottom waters by correcting the $\delta^{18}O_{benthic}$ record for sub-surface temperature using TEX_{86} and compared this to the hydrogen isotopic composition of surface seawater reconstructed based on the $\delta^2H_{C37:2}$ record. Our results shed new light on the evolution of seawater isotopic compositions in the eastern North Atlantic during the Middle Miocene.

2. Materials and Methods

2.1. Geographic Setting

The Integrated Ocean Drilling Program (IODP) drilling site U1318 is located at coordinates 51°26.16'N, 11°33.0'W, with a water depth of 409 m (Expedition 307 Scientists, 2006). The paleolatitude during the Middle Miocene (~15 Ma) was ~47°N (Van Hinsbergen et al., 2015) at a similar water depth as today (Ryan et al., 2009), situated on the upper slope edge of the continental margin within the Porcupine Seabight (Figure 1). The seabight represents a failed rift system that originated during the Middle to Late Jurassic period when the North Atlantic Ocean was being formed. During the Middle Miocene epoch (16–11.7 million years; Cohen et al., 2013), the British Isles were still connected to continental Europe, with no connection to the North Sea (Gibbard & Lewin, 2003). The Porcupine Basin is filled with approximately 12 km of sedimentary deposits ranging from the Late Paleozoic era to the Quaternary period (Ryan et al., 2009). These sediments primarily originate from the Irish and Celtic shelves (Rice et al., 1991). Present-day surface water temperatures (SST) at Site U1318 show a seasonal variation, ranging from ca. 10°C during winter to around 16°C during summer (Locarnini et al., 2018). However, at depths below ca. 50 m, the water temperature remains constant throughout the year at approximately 11°C (Locarnini et al., 2018; Sangiorgi et al., 2018). The core location and Porcupine bank is under the influence of the Continental Slope Current (CSC). The CSC transports Eastern North Atlantic Water via the North Atlantic Current (NAC) to the Norwegian Sea (Raddatz et al., 2011). The present-day annual mean salinity of the surface layer (0–50 m) at the core location area is 34.9–35.5 psu (Zweng et al., 2018).
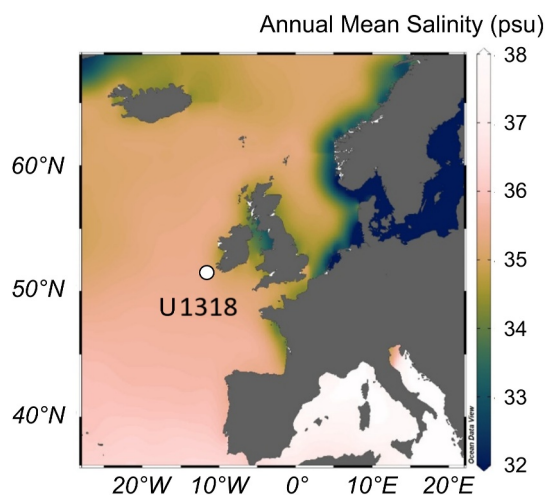
Figure 1. Map of sea surface salinity data from Zweng et al. (2018) using a scientific color map from Crameri (2023) showing the sediment core location. U1318 core was drilled in the Porcupine Basin which is at the Northeast Atlantic shelf.

2.2. Age Model

To target the Middle Miocene, samples were collected from Site U1318 Hole B (cores 10H–14H and 17X–27X) and Hole C (cores 7H and 8X–10X, Expedition 307 Scientists, 2006) between 92.4 and 247.5 m composite depth (mcd). The age model for this depth interval is based on integrated bio-, isotope- and magnetostratigraphy, as presented in Quaijtaal et al. (2018). Two hundred forty-five (245) samples were previously analysed for $U_{37}^{K'}$ and TEX$_{86}$ proxies (Sangiorgi et al., 2021) from which 145 samples had sufficient material for stable oxygen and carbon isotopes analysis of the benthic foraminifera *Uvigerina sp.* and *Cibicidoides pachyderma* (Quaijtaal et al., 2018). The Middle Miocene samples consist mainly of greenish-gray clay with total organic carbon content ranging between 0.27% and 0.70% (Sangiorgi et al., 2021). The samples between 92.4 and 247.5 mcd cover the age interval 12.75–16.60 Ma with an average time resolution of 25 kyrs for stable carbon and oxygen isotope analysis and 17 kyrs for organic geochemistry. To increase the resolution of the organic geochemistry and hydrogen isotope record we extracted 25 additional samples between 98.05 and 230.42 mbsf following the extraction and fractionation procedures of Sangiorgi et al. (2021). The average time resolution for the extended organic geochemistry record is 14 and 31 kyrs for the hydrogen isotope record.

2.3. Long-Chain Alkenones and GDGT Analysis

Alkenones and glycerol dialkyl glycerol tetraethers (GDGTs) were extracted and analysed as previously described by Sangiorgi et al. (2021). Furthermore, we re-analysed all GDGT fractions with improved analytical methodology (Hopmans et al., 2016) using an ultra-high performance liquid chromatography/mass spectrometry (UHPLC/MS) on an Agilent 1,260 Infinity HPLC 230 coupled to Agilent 6130 MSD using two silica BEH HILIC columns (2.1 mm × 150 mm, 1.7 μm 232 thickness) connected in series and maintained at 25°C. A solvent gradient of hexane/isopropanol (9:1, v/v) (solvent A) and hexane (solvent B) was used starting with 18% of solvent A and 82% of solvent B at a constant flow rate of 0.2 ml/min. The GDGTs were eluted isocratically for 25 min and thereafter solvent A increased in a linear gradient to 30% in 25 min and to 100% of solvent A in the following 30 min. GDGTs were detected in Selective Ion Monitoring (SIM) mode for protonated GDGT molecules [M+H]$^+$. The TEX$_{86}$ index was calculated after Schouten et al. (2002) and the calibration against the average subsurface temperature between 0 and 200 m (subT) is from Kim et al. (2012) (Equations 1 and 2) with a standard error of ±2.2°C.

$$\text{TEX}_{86}^H = \log(\text{TEX}_{86}) \tag{1}$$

$$\text{sub}T = 54.7 * \text{TEX}_{86}^H + 30.7 \tag{2}$$

The alkenones of the ketone fractions of the 25 additional samples taken in the study were measured using an Agilent 6890°N gas chromatograph coupled to a flame ionization detector (GC-FID), equipped with a CP Sil-5 fused silica capillary column (50 m × 0.32 mm, 0.12 μm thickness), to determine the quality of the fraction for further isotope analysis and to calculate the $U_{37}^{K'}$ values (Equation 3) according to Prahl & Wakeham (1987). The $U_{37}^{K'}$-based SSTs were calculated with the global core-top calibration of Müller et al. (1998) (Equation 4).

$$U_{37}^{K'} = \frac{[C_{37:2}]}{[C_{37:2}] + [C_{37:3}]} \tag{3}$$

$$\text{SST} = \frac{U_{37}^{K'} - 0.044}{0.033} \tag{4}$$

Hydrogen isotope ratios of alkenones of 124 fractions (99 from the original sample set of Sangiorgi et al. (2021) and 25 additional samples) were measured in duplicate using a gas chromatograph coupled to a Thermo Delta V

isotope ratio mass spectrometer via high-temperature conversion reactor (Isolink I) and Conflo IV. The GC was equipped with an RTX–200 60 m column according to Weiss et al. (2019) and samples were injected manually. We report the δ^2H ratio of alkenone $C_{37:2}$ determined by manual peak integration. $C_{37:2}$ appears as the main alkenone peak, while $C_{37:3}$ and C_{38} alkenone peaks are in lower relative abundance and most of the time below minimal intensity for the isotope ratio integration. We report the $\delta^2 H_{C37:2}$ value as average value of the replicate analysis together with the standard deviation. Standard deviations for δ^2H ratios represent the reproducibility between replicate analytical runs, and generally fall within the 3‰ precision window for the Thermo Scientific Delta V. The analytical error of the $\delta^2 H_{C37:2}$ measurements is 2.4‰ based on the pooled standard error of 273 $\delta^2 H_{C37:2}$ measurement runs. The hydrogen isotope values for alkenones were standardized against pulses of H_2 reference gas, which was injected three times at the beginning and two times at the end of each run. Daily, before running samples, the H_3^+ factor was measured and the day-to-day variability was never more than 0.5 ppm/nA, and the performance and stability of the machine was monitored by measuring an n-alkane standard, Mix B (supplied by A. Schimmelmann, Indiana University). The n-alkanes mixture covers a δ^2H range from approximately −9‰ to −264‰ and intensities ranging from 1,000 to 4,000 mV. Samples were only run when the average difference and standard deviation between online and certified values was less than 5‰. The average pooled standard deviation of the n-alkanes in 67 Mix B runs is 4.7‰. To further monitor the system performance squalene and C_{30} n-alkane were co-injected with each sample with measured values ranging from −161 ± 11‰ to −74 ± 6‰. The offline predetermined values are −170 ± 4‰ for squalene and −79 ± 5‰ for C_{30} n-alkane. The larger standard deviations and offsets compared to offline values are due to compounds in ketone fractions of these samples that co-elute with the co-injected standards.

2.4. Calculation of Seawater Isotopes

For the calculation of $\delta^2 H_{SSW}$ from the hydrogen isotopic composition of $C_{37:2}$ we applied the open-ocean relationship based on surface ocean suspended particulate organic material (SPOM) by Gould et al. (2019) (Data Set S2 in Supporting Information S1):

$$\delta^2 H_{C37} = 1.48\ (\pm 0.4) \times \delta^2 H_{SSW} - 199\ (\pm 3)\ (RMSE = 5.8‰) \tag{5}$$

We reconstructed the oxygen isotopic composition of the bottom seawater ($\delta^{18} O_{BSW}$) from the benthic foraminifera δ^{18}O data set published in Quaijtaal et al. (2018) which consists of δ^{18}O values of *Cibicidoides pachyderma* and δ^{18}O values of *Uvigerina sp* converted to *C. pachyderma*. For the temperature correction we used the updated and extended records of $U_{37}^{K'}$ and TEX^H_{86} (Data Set S1 in Supporting Information S1). We calculated the $\delta^{18} O_{BSW}$ with the relationship described by Lynch-Stieglitz et al. (1999) as arranged by Cramer et al. (2011) (Equations 6 and 7). We report $\delta^{18} O_{BSW}$ values in VSMOW with the accepted conversion value of 0.27‰ (VPDB to VSMOW) (Equations 6 and 7) (Cramer et al., 2011). The uncertainty in the parameters in this equation are poorly constrained and likely relatively small compared to the uncertainties in the temperature estimations. The pooled standard error (analytical error) of the $\delta^{18} O_{benthic}$ analyses is 0.06‰.

$$t = 16.1 - 4.76 \times \left(\delta^{18} O_{benthic} - \left(\delta^{18} O_{BSW} - 0.27\right)\right) \tag{6}$$

Rearranged to $\delta^{18} O_{BSW}$:

$$\delta^{18} O_{BSW} = \frac{-16.1 + 4.76 \times \delta^{18} O_{benthic} + t}{4.76} + 0.27 \tag{7}$$

The modern open-ocean relationship between oxygen and hydrogen isotopes is described by Hättig et al. (2023) as the modern open-ocean waterline (MOOWL) and is based on the data sets of Gould et al. (2019), Rohling (2007), Srivastava et al. (2010) and Weiss et al. (2019) and the Water isotope Database (2022) managed by Dr. G. Bowen (University of Utah):

$$\delta^2 H_{SW} = 6.58 \times \delta^{18} O_{SW} - 0.12\ (RMSE = 1.1‰) \tag{8}$$

Rearranged to $\delta^{18} O_{SW}$:

$$\delta^{18}O_{SW} = 0.152 \times \delta^2H_{SW} - 0.018 \quad (RMSE = 0.17\text{‰}) \tag{9}$$

For the error propagation we use the analytical error based on the pooled standard error of δ^2H_{C37} instead of the external standard Mix B as the latter compromises a different class of compounds (*n*-alkanes), with a much larger range of intensities and isotope values than the C_{37} alkenones explaining their larger SE. Furthermore, they elute at different backgrounds and column temperatures. The propagated error for reconstructing changes in δ^2H_{SSW} is 3.4‰, resulting from the combination of the pooled standard error of δ^2H_{C37} and the error of the slope of Equation 5. The propagated error for absolute δ^2H_{SSW} values is 6.3‰, resulting from the pooled standard error of δ^2H_{C37} and the root-mean-square error of Equation 5. The propagated error for absolute δ^2H_{BSW} values and changes in δ^2H_{BSW} is 1.2‰, resulting from the analytical error of oxygen isotopes, an uncertainty of 2.2°C in TEX_{86} subsurface temperature reconstruction and the error in the waterline calibration (Equation 8). The propagated error for $\delta^{18}O_{BSW}$ is 0.46‰. Note that for Equation 6 no root-mean-square error is reported and thus the propagated error for $\delta^{18}O_{BSW}$ and δ^2H_{BSW} is likely underestimated.

3. Results and Discussion

3.1. Temperature Records

The reanalysis of GDGT fractions of IODP core U1318B using updated methodology (Hopmans et al., 2016) resulted in slightly shifted TEX^H_{86} values by on average −0.01 compared to those published by Sangiorgi et al. (2021), with some values changing by up to 0.06 due to the better separation of GDGTs, especially the GDGT-2 peak (Figure S1b in Supporting Information S1). In contrast to Sangiorgi et al. (2021), we converted the TEX^H_{86} values to subsurface temperature (subT; the average of 0–200 m temperatures as defined by Kim et al., 2012) values as we aim to ultimately use the temperature estimates to correct the $\delta^{18}O_{benthic}$ values (see below). The subT record varies between 13°C and 21°C (Figure 2) and shows the same cooling trends described by Sangiorgi et al. (2021) for the SST inferred from TEX^H_{86}. The recalculated BIT index is below 0.3 in all samples, in good agreement with Sangiorgi et al. (2021), suggesting no bias on TEX_{86} values by continental organic matter input (Figure S1b in Supporting Information S1). The GDGT-2/GDGT-3 ratio (Taylor et al., 2013) is relatively constant between 1.7 and 3.2, suggesting that GDGTs are consistently from shallow depths (Hurley et al., 2018; Kim et al., 2015; Taylor et al., 2013) as expected in this relatively shallow water location of ca. 409 m depth. Furthermore, Varma et al. (2023) showed that the TEX_{86} signal is mainly from depths shallower than 350 m. Finally, present day temperatures between 50 and approximately 500 m water depth are quite constant (Locarnini et al., 2018; Wienberg et al., 2020). Based on this, we use the 0–200 m calibration of Kim et al. (2012) to calculate subT, but in Figures S5 and S6 of Supporting Information S1 we also present an alternative temperature reconstruction using the 0–400 m calibration of Ho and Laepple (2016). The extended $U^{K'}_{37}$-based SST record is on average 4–8°C higher than the subT estimated from TEX^H_{86} with temperatures varying between 25.8 and 28.9°C (Figure 2) and a cooling of ca. 3°C between 14.6 and 12.7 Ma. Thus the $U^{K'}_{37}$ reflects a similar temperature trend as TEX^H_{86}, but with a smaller amplitude, which is surprising as bottom water temperatures typically vary to a smaller degree then SST. This difference is likely due to the $U^{K'}_{37}$ reaching its maximum value of 1 (cf. Sangiorgi et al., 2021) and thus this proxy is unable to record SST higher than 29°C which may have been present during the first part of the Middle Miocene record.

3.2. Evolution of Oxygen Isotopes of Bottom Water

The oxygen isotope ratio of benthic *Cibicidoides pachyderma* as published by Quaijtaal et al. (2018) follows the trend of the global benthic stack (Westerhold et al., 2020, CENOGRID). During the MMCO between 16.6 and 14.59 Ma, the $\delta^{18}O_{benthic}$ signal varies between −0.35 and 0.58‰ with an average value of 0.12 ± 0.23‰. During the MMCT from 14.59 to 12.75 Ma, values increase as high as 1.43‰. This ca. 1‰ increase is similar to what is observed in the global $\delta^{18}O_{benthic}$ stack record and has until recently been associated with ice volume increase (Billups & Schrag, 2002; Haq et al., 1987; Rohling et al., 2022). Recent studies, however, suggest a strong bottom water cooling explaining most of the increase in $\delta^{18}O_{benthic}$, and therefore little to no ice volume build up (Hou et al., 2023; Leutert et al., 2021; Meckler et al., 2022; Modestou et al., 2020).

Several Mi-events were tentatively identified based on positive oxygen isotope excursions linked to magneto-stratigraphy and palynology changes (Quaijtaal et al., 2014, 2018; Sangiorgi et al., 2021). In particular Mi-events
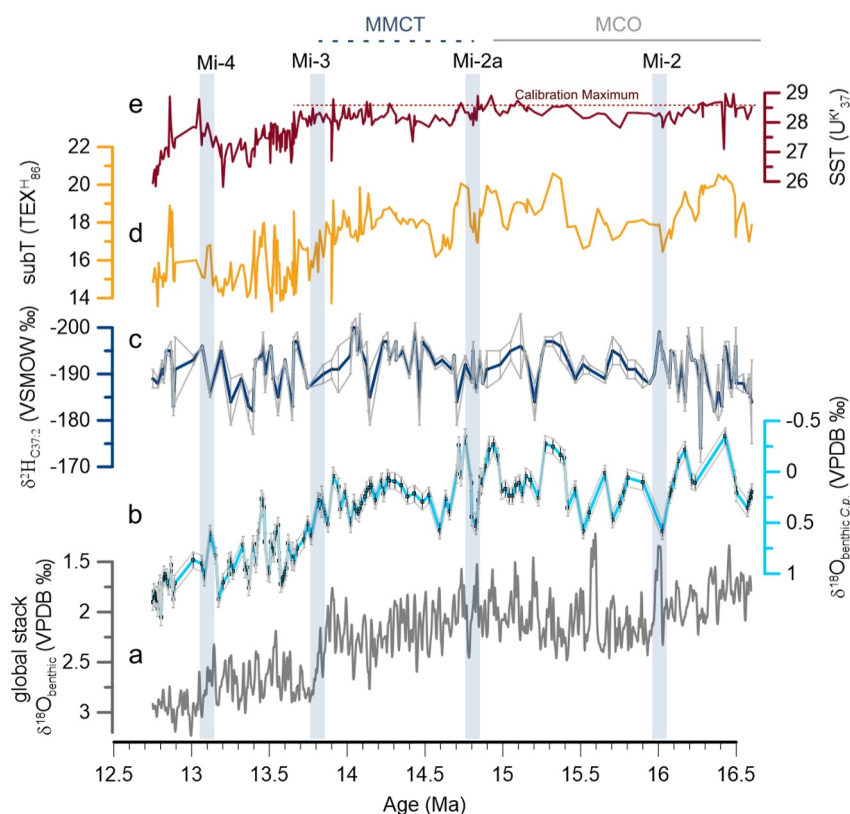
Figure 2. Middle Miocene multiproxy temperature and seawater isotope record, Site U1318. Globally recognized Miocene cooling events (Mi-events; Miller et al., 1991; Steinthorsdottir et al., 2021) are marked with blue bars and were identified by Quaijtaal et al. (2014) based on a sharp increase in $\delta^{18}O_{benthic}$ in combination with palynology and magnetostratigraphy. (a) Global stack $\delta^{18}O$ of benthic foraminifera (CENOGRID, Westerhold et al., 2020); (b) local oxygen isotope data of *Cibicidoides pachyderma* (*C.p.*) (Quaijtaal et al., 2018), error bars represent the standard deviation of duplicate isotope measurements; (c) $\delta^{2}H$ of long-chain alkenones $C_{37:2}$ (this study), error bars represent the standard deviation of duplicate isotope measurements; (d) revised subsurface temperature (subT) based on TEX^{H}_{86} index calculated with Kim et al. (2012) (this study); (e) surface temperature (SST) based on $U^{K'}_{37}$ index (Sangiorgi et al., 2021). The age model is presented in Quaijtaal et al. (2018).

2, 2a and 3 are likely reflected in the local $\delta^{18}O_{benthic}$ with positive excursions of ca. 0.8‰. The Mi-2a event (ca. 14.8 Ma) is linked to an eustatic sea level fall of ca. 30 m and a cooling of ca. 0.7°C in deep waters (John et al., 2011; Miller et al., 2020) and the Mi-3 event (13.8 Ma) is associated with cooling in the deep ocean of 1.2°C and ca. 50 m eustatic sea level fall (De Vleeschouwer et al., 2017; Miller et al., 2020) and a pCO_2 decline from ca. 600 to 400–500 ppm (Sosdian & Lear, 2020). The global Mi-4 (Steinthorsdottir et al., 2021) is less pronounced in our local record with a small increase of ca. 0.3‰.

To reconstruct $\delta^{18}O_{BSW}$ from benthic foraminifera we need to reconstruct bottom water temperatures (e.g., Hou et al., 2023; Lear et al., 2015; Modestou et al., 2020). Unfortunately, we were not able to do this using benthic foraminifera. However, the core location is at a rather shallow water depth of ca. 409 m with present day relatively small temperature differences between bottom waters and subsurface (0–200 m) waters of 1–3°C (Figure S2 in Supporting Information S1, Locarnini et al., 2018; Sangiorgi et al., 2021). Therefore, we corrected $\delta^{18}O_{benthic}$ with the subT derived from TEX^{H}_{86}. The reconstructed $\delta^{18}O_{BSW}$ values range between 0.6 and 1.4‰, a similar range as reconstructed by Hou et al. (2023) for the Middle Miocene at the Southern Hemisphere deep-ocean Site 1,168. Interestingly, our reconstructed bottom water oxygen isotope record shows no increasing trend between 14.5 and 13.5 Ma and only a minor increase of ca. 0.2‰ after 13.5 Ma (Figure 3a; see Supporting Information S1 for further discussion). This suggests no major change in seawater isotopic compositions after 14.6 Ma at least for this core location in the eastern North Atlantic, in agreement with the suggestion of Sangiorgi et al. (2021) that benthic oxygen isotopes of U1318 are mainly controlled by temperature at this core location.
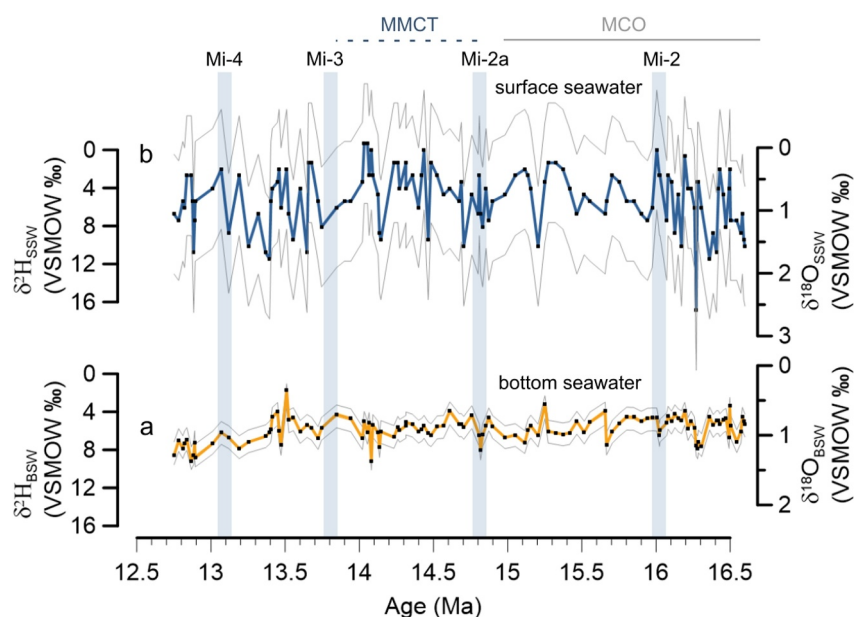
Figure 3. Seawater isotope reconstruction. (a) Bottom seawater isotopes are reconstructed with oxygen isotopes of foraminifera: $\delta^{18}O_{BSW}$ is calculated with Cramer et al. (2011) and subT from the same sediment depth signal. $\delta^{18}O_{BSW}$ was translated with the modern open-ocean waterline (MOOWL) to $\delta^{2}H_{BSW}$. Gray lines indicate the propagated error of 1.2‰ for $\delta^{2}H_{BSW}$. (b) The surface seawater isotope reconstruction is based on hydrogen isotope analysis of $C_{37:2}$ alkenones, $\delta^{2}H_{SSW}$ is calculated with the SPOM calibration from Gould et al. (2019) and translated to $\delta^{18}O_{SSW}$ with the MOOWL (Equation 8). Gray lines indicate the propagated error of 6.3‰ for absolute $\delta^{2}H_{SSW}$. Note that the error for changes in $\delta^{2}H_{SSW}$ is 3.4‰ (see main text). Global Miocene cooling events (Mi-events; Miller et al., 1991; Steinthorsdottir et al., 2021) are marked with blue bars and are identified by Quaijtaal et al. (2014) based on a sharp increase in $\delta^{18}O_{benthic}$ in combination with palynology and magnetostratigraphy.

Regarding the short-term Mi-events, during Mi-2 and Mi-2a the reconstructed $\delta^{18}O_{BSW}$ shows a sharp excursion of 0.3‰ while Mi-3 and Mi-4 show a stepwise increase of 0.2–0.3‰. However, it is difficult to distinguish those events from the large variability in the record which can be up to 0.5‰.

3.3. Evolution of Hydrogen Isotopes of Surface Water

The $\delta^{2}H_{C37:2}$ values of the Middle Miocene sediment record at Site U1318 ranges between −200‰ and −172‰ (Figure 2c). In contrast to the $\delta^{18}O_{benthic}$ and subT record (Figure 2d), the $\delta^{2}H_{C37:2}$ record shows no substantial increase between 14.6 and 12.75 Ma. Between 15.5 and 15.2 Ma $\delta^{2}H_{C37:2}$ decreases parallel to the $\delta^{18}O_{benthic}$ record from −190‰ to −195‰, followed by a sharp increase to −186‰. But, during the global cooling step and Mi-3 event $\delta^{2}H_{C37:2}$ increases first continuously from −200‰ at 14.1 Ma to −187‰ at 13.7 Ma, then decreases sharp to −195‰ and continues to vary. Due to the large variability we were not able to rigorously identify the Mi-events in the $\delta^{2}H_{C37:2}$ record.

The $\delta^{2}H_{C37:2}$ alkenone record was subsequently converted into a $\delta^{2}H_{SSW}$ record using the calibration of Gould et al. (2019) (Equation 5). This assumes that the alkenones are mainly derived from open-ocean haptophyte species. However, little is known about haptophyte species during the Miocene. The main producer may have been *Reticulofenestra* (Perch-Nielsen, 1985; Samtleben, 1980), ancestor of the present day open-ocean species *Emiliania huxleyi* (Gibbs et al., 2013). We observed a typical open-ocean alkenone distribution with a dominant abundance of the $C_{37:2}$ next to C_{38} suggesting that open-ocean haptophytes (Type III; Kleijne, 1993) were the dominant alkenone producers at the time.

Conversion of the $\delta^{2}H_{C37:2}$ alkenone values resulted in $\delta^{2}H_{SSW}$ values ranging between −1 and +17‰ (Figure 3b). The average $\delta^{2}H_{SSW}$ for this record is 5.2 ± 3.1‰, which is similar to the nearest (ca. 313 km distance from the core site) modern measured $\delta^{2}H$ value of surface seawater, +2.1‰ (Gould et al., 2019). Similar to the $\delta^{2}H_{C37:2}$ record there is no increase in $\delta^{2}H_{SSW}$ after 14.8 Ma, in contrast to the $\delta^{18}O_{benthic}$ and subT records. During the Mi-events, $\delta^{2}H_{SSW}$ seemingly increased by 2–6‰, but these events cannot be clearly distinguished

due to the large overall variability, similar to the reconstructed $\delta^{18}O_{BSW}$. Thus, reconstructed δ^2H_{SSW} and $\delta^{18}O_{BSW}$ records both show a lack of any substantial increase in isotope values between 14.6 and 12.75 Ma, although $\delta^{18}O_{BSW}$ does show a small increase after 13.5 Ma. These two independent records thus suggest that this period, the Miocene Climate Transition (MMCT; 14.7–13.8 Ma) was not associated with a substantial change in the isotopic composition of seawater in the eastern North Atlantic.

4. Implications

Our record of reconstructed hydrogen isotopic composition of surface seawater, based on an approach not requiring any temperature correction, clearly shows that the MMCT was not associated with a strong change in seawater isotopic composition, suggesting that the change in oxygen isotopic composition of benthic foraminifera was mainly reflecting a substantial cooling of 4–5°C in the eastern North Atlantic Ocean. The question arises whether this phenomenon is unique for this location or whether it is a global phenomenon. Interestingly, our results agree with recent studies based on clumped isotope data of benthic foraminifera which suggest higher than previously estimated bottom water temperatures during the MMCO and indicate strong bottom water cooling during the MMCT (Hou et al., 2023; Leutert et al., 2021; Meckler et al., 2022; Modestou et al., 2020). Their inferred cooling of ca. 5°C could in principle completely explain the global Middle Miocene $\delta^{18}O_{benthic}$ evolution and implies a stable ice volume and thus little to no ice volume buildup (Hou et al., 2023). Our results confirm Middle Miocene stable seawater isotopic composition for both δ^2H and $\delta^{18}O$ suggesting no ice volume buildup. This contrasts with geological reconstructions of ice sheet advances during those time periods (e.g., Fielding et al., 2011; Hauptvogel & Passchier, 2012; Levy et al., 2016; Passchier et al., 2011). However, as suggested by Hou et al. (2023) the progressive Neogene Southern Ocean ice volume could be explained by a progressively lowering of Antarctic ice sheet height while the ice expands seawards during the Middle Miocene. The total global ice volume might have been stable, but the volume to area ratio might have changed (Hou et al., 2023). This million year MMCT cooling caused by the decrease in pCO_2 (Pagani et al., 1999; Super et al., 2018) may thus have led to similar global ice volumes coupled with deep ocean cooling.

Translation of our average reconstructed hydrogen isotopic compositions of surface seawater ($\delta^2H_{SSW} = 5.2 \pm 3.1$‰) to $\delta^{18}O_{SSW}$ using the MOOWL suggests values of ca. 0.8 ± 0.5‰, similar to $\delta^{18}O_{BSW} = 0.9 \pm 0.2$‰ based on foraminifera. This suggests relatively small differences between bottom and surface seawater isotopes. Furthermore, similar to Hou et al. (2023) the reconstructed surface and bottom seawater isotopes fall in the range of the modern open-ocean seawater isotopic composition ($\delta^{18}O = -0.5$ and 1.5‰, $\delta^2H = 0$–10‰, LeGrande et al., 2006; Rohling, 2007; Hättig et al., 2023). This may imply similar ice volumes in the MMCT as those of modern day (Hou et al., 2023; Rohling et al., 2022).

During the Middle Miocene there were several short-lived (ca. 100 kyr) $\delta^{18}O_{benthic}$ increases thought to be associated with BWT decreases of 0.7–1.2°C and attendant sea-level falls of 20–50 m: Mi-2 (16 Ma), Mi-2a (14.8 Ma), Mi-3 (13.8 Ma), and Mi-4 (13.1 Ma) (Holbourn et al., 2013; Miller et al., 2020). However, both our reconstructed $\delta^{18}O_{BSW}$ and δ^2H_{SSW} values do not consistently show these excursions mainly due to the large overall variability in our records. For our δ^2H_{SSW} record, this variability may be caused by the analytical uncertainty of compound-specific hydrogen isotope analysis, for example, the pooled standard error of analysis is ca. 2.4‰. Furthermore, variable fractionation factors between alkenones and water for different species (e.g., Schouten et al., 2006; M'Boule et al., 2014; van der Meer et al., 2015; Wolhowe et al., 2015) may lead to incorrect estimates of δ^2H_{SSW} while the calibration error between δ^2H_{C37} and δ^2H_{SSW} is also relatively large (root-mean-square error of 5.8‰ for the calibration of Gould et al., 2019), hinting at factors other than δ^2H_{SSW} impacting δ^2H_{C37} such as light intensity and nutrient availability (e.g., Sachs et al., 2017; van der Meer et al., 2015; Weiss et al., 2017; Wolfshorndl et al., 2019; Wolhowe et al., 2015). Using the analytical error and the error of the calibration slope we determined that the hydrogen isotopic composition of alkenones can detect changes in δ^2H_{SSW} exceeding 3–4‰, potentially corresponding to $\delta^{18}O_{SSW}$ fluctuations >0.5‰. Our reconstructed $\delta^{18}O_{BSW}$ may be impacted by incorrect estimations of subsurface water TEX^H_{86} estimates. Furthermore, the $\delta^{18}O_{benthic}$ record may be influenced by diagenetic alteration (e.g., Corfield et al., 1990; Pearson et al., 2001, 2007; Sexton & Wilson, 2009) and bioturbation (e.g., Hülse et al., 2022). Quaijtaal et al. (2018) did observe minor secondary crystals on the shell walls which might have influenced the isotopic values. Clearly it would be beneficial to generate hydrogen isotope records from different sites, including equatorial and Southern Ocean sites, to reconstruct the global surface seawater isotope distribution and evolution and potentially disentangle which isotope events (Mi-events) were caused by cooling or a combination of cooling and seawater isotopic composition

change. Nevertheless, our results have shown potential for $\delta^2 H_{C37}$ records in the Cenozoic to provide seawater isotope records which are independent from temperature.

5. Conclusions

We presented a high-resolution Middle Miocene hydrogen isotope record of alkenones from a shelf site (U1318) in the Porcupine basin, in eastern North Atlantic. Our record reflects no long-term changes in surface seawater isotopes during the MMCT. Calculated bottom seawater isotopes based on benthic oxygen isotopes and sub-surface TEX^H_{86} temperature correction also indicate no long-term change during this period. This suggests a fairly stable seawater isotopic composition during the MMCT for both bottom and surface waters at this shallow (409 m) site, suggesting no or a very limited ice volume effect on seawater isotopic composition and indicating that the Miocene Climate Transition was mainly a time of cooling. More independent seawater isotope records of the Atlantic and Pacific Ocean covering the MMCT are needed to confirm if this was a global phenomenon.

Data Availability Statement

Data is available at PANGAEA (Hättig et al., 2024). All processed sediment samples are stored at NIOZ, that is, TLE, apolar, ketone, polar fractions of U1318. All unprocessed raw data files are archived in the NIOZ data archive system (DAS) and available upon request by contacting DAS@nioz.nl.

References

Badger, M. P. S., Lear, C. H., Pancost, R. D., Foster, G. L., Bailey, T. R., Leng, M. J., & Abels, H. A. (2013). CO_2 drawdown following the middle Miocene expansion of the Antarctic Ice Sheet. *Paleoceanography*, 28(1), 42–53. https://doi.org/10.1002/palo.20015

Billups, K., & Schrag, D. P. (2002). Paleotemperatures and ice volume of the past 27 Myr revisited with paired Mg/Ca and $^{18}O/^{16}O$ measurements on benthic foraminifera. *Paleoceanography*, 17(1), 3-1-3–11. https://doi.org/10.1029/2000pa000567

Billups, K., & Schrag, D. P. (2003). Application of benthic foraminiferal Mg/Ca ratios to questions of Cenozoic climate change. *Earth and Planetary Science Letters*, 209(1–2), 181–195. https://doi.org/10.1016/S0012-821X(03)00067-0

Chivall, D., M'Boule, D., Sinke-Schoen, D., Sinninghe Damsté, J. S., Schouten, S., & van der Meer, M. T. J. (2014). The effects of growth phase and salinity on the hydrogen isotopic composition of Alkenones produced by coastal haptophyte algae. *Geochimica et Cosmochimica Acta*, 140, 381–390. https://doi.org/10.1016/j.gca.2014.05.043

Cohen, K. M., Finney, S. C., Gibbard, P. L., & Fan, J.-X. (2013). The international chronostratigraphic chart. *Episodes*, 36(3), 199–204. https://doi.org/10.18814/epiiugs/2013/v36i3/002

Corfield, R. M., Hall, M. A., & Brasier, M. D. (1990). Stable isotope evidence for foraminiferal habitats during the during of the Cenomanian/Turonian ocean anoxic event. *Geology*, 18(2), 175–178. https://doi.org/10.1130/0091-7613(1990)018%3C0175:SIEFFH%3E2.3.CO;2

Cramer, B. S., Miller, K. G., Barrett, P. J., & Wright, J. D. (2011). Late Cretaceous-Neogene trends in deep ocean temperature and continental ice volume: Reconciling records of benthic foraminiferal geochemistry ($\delta^{18}O$ and Mg/Ca) with sea level history. *Journal of Geophysical Research*, 116(12), C12023. https://doi.org/10.1029/2011JC007255

Cramer, B. S., Toggweiler, J. R., Wright, J. D., Katz, M. E., & Miller, K. G. (2009). Ocean overturning since the Late Cretaceous: Inferences from a new benthic foraminiferal isotope compilation. *Paleoceanography*, 24(4), PA421. https://doi.org/10.1029/2008PA001683

Crameri, F. (2023). Scientific color maps (8.0.0) [Dataset]. *Zenodo*. https://doi.org/10.5281/zenodo.5501399

De Vleeschouwer, D., Vahlenkamp, M., Crucifix, M., & Pälike, H. (2017). Alternating Southern and Northern Hemisphere climate response to astronomical forcing during the past 35 m.y. *Geology*, 45(4), 375–378. https://doi.org/10.1130/G38663.1

Elderfield, H., Ferretti, P., Greaves, M., Crowhurst, S., McCave, I. N., Hodell, D., & Piotrowski, A. M. (2012). Evolution of ocean temperature and ice volume through the mid-Pleistocene climate transition. *Science*, 337(6095), 704–709. https://doi.org/10.1126/science.1221294

Expedition 307 Scientists. (2006). Site U1318. In T. G. Ferdelman, A. Kano, T. Williams, & J. P. Henriet, (Eds.), *Proceedings of the Integrated Ocean Drilling Program* (Vol. 307, pp. 1–57). Integrated Ocean Drilling Program Management International. https://doi.org/10.2204/iodp.proc.307.105.2006

Fielding, C. R., Browne, G. H., Field, B., Florindo, F., Harwood, D. M., Krissek, L. A., et al. (2011). Sequence stratigraphy of the Andrill AND-2A Drillcore, Antarctica: A long-term, ice-proximal record of early to mid-Miocene climate, sea-level and glacial dynamism. *Palaeogeography, Palaeoclimatology, Palaeoecology*, 305(1), 337–351. https://doi.org/10.1016/j.palaeo.2011.03.026

Gibbard, P. L., & Lewin, J. (2003). The history of the major rivers of southern Britain during the Tertiary. *Journal of the Geological Society*, 160(6), 829–845. https://doi.org/10.1144/0016-764902-137

Gibbs, S. J., Poulton, A. J., Bown, P. R., Daniels, C. J., Hopkins, J., Young, J. R., et al. (2013). Species-specific growth response of coccolithophores to Palaeocene–Eocene environmental change. *Nature Geoscience*, 6(3), 218–222. https://doi.org/10.1038/ngeo1719

Goldner, A., Herold, N., & Huber, M. (2014). Antarctic glaciation caused ocean circulation changes at the Eocene-Oligocene transition. *Nature*, 511(7511), 574–577. https://doi.org/10.1038/nature13597

Gould, J., Kienast, M., Dowd, M., & Schefuß, E. (2019). An open-ocean assessment of Alkenone δD as a paleo-salinity proxy. *Geochimica et Cosmochimica Acta*, 246, 478–497. https://doi.org/10.1016/j.gca.2018.12.004

Greenop, R., Foster, G. L., Wilson, P. A., & Lear, C. H. (2014). Middle Miocene climate instability associated with high-amplitude CO_2 variability. *Paleoceanography*, 29(9), 845–853. https://doi.org/10.1002/2014PA002653

Haq, B. U., Hardenbol, J., & Vail, P. R. (1987). Chronology of fluctuating sea levels since the Triassic. *Science*, 235(4793), 1156–1167. https://doi.org/10.1126/science.235.4793.1156

Hättig, K., Varma, D., Louwye, S., Schouten, S., & van der Meer, M. T. J. (2024). Hydrogen isotopes and revised SST of middle Miocene seawater from IODP site 307-U1318 [Dataset]. *PANGAEA*. https://doi.org/10.1594/PANGAEA.967157

Hättig, K., Varma, D., Schouten, S., & van der Meer, M. T. J. (2023). Glacial-interglacial sea water isotope change near the Chilean Margin as reflected by δ^2H of C37 alkenones. *Climate of the Past*, *19*, 1919–1930. https://doi.org/10.5194/cp-19-1919-2023

Hauptvogel, D. W., & Passchier, S. (2012). Early–Middle Miocene (17–14Ma) Antarctic ice dynamics reconstructed from the heavy mineral provenance in the AND-2A drill core, Ross Sea, Antarctica. *Global and Planetary Change*, *82–83*, 38–50. https://doi.org/10.1016/j.gloplacha.2011.11.003

Ho, S., & Laepple, T. (2016). Flat meridional temperature gradient in the early Eocene in the subsurface rather than surface ocean. *Nature Geoscience*, *9*(8), 606–610. https://doi.org/10.1038/ngeo2763

Holbourn, A., Kuhnt, W., Clemens, S., Prell, W., & Andersen, N. (2013). Middle to late Miocene stepwise climate cooling: Evidence from a high-resolution deep water isotope curve spanning 8 million years. *Paleoceanography*, *28*(4), 688–699. https://doi.org/10.1002/2013PA002538

Hopmans, E. C., Schouten, S., & Sinninghe Damsté, J. S. (2016). The effect of improved chromatography on GDGT-based Palaeoproxies. *Organic Geochemistry*, *93*, 1–6. https://doi.org/10.1016/j.orggeochem.2015.12.006

Hou, S., Stap, L. B., Paul, R., Nelissen, M., Hoem, F. S., Ziegler, M., et al. (2023). Reconciling Southern Ocean fronts equatorward migration with minor Antarctic ice volume change during Miocene cooling. *Nature Communications*, *14*(1), 7230. https://doi.org/10.1038/s41467-023-43106-4

Hülse, D., Vervoort, P., van de Velde, S. J., Kanzaki, Y., Boudreau, B., Arndt, S., et al. (2022). Assessing the impact of bioturbation on sedimentary isotopic records through numerical models. *Earth-Science Reviews*, *234*, 104213. https://doi.org/10.1016/j.earscirev.2022.104213

Hurley, S. J., Lipp, J. S., Close, H. G., Hinrichs, K. U., & Pearson, A. (2018). Distribution and export of isoprenoid Tetraether lipids in suspended particulate matter from the water column of the Western Atlantic Ocean. *Organic Geochemistry*, *116*, 90–102. https://doi.org/10.1016/j.orggeochem.2017.11.010

John, C. M., Karner, G. D., Browning, E., Leckie, R. M., Mateo, Z., Carson, B., et al. (2011). Timing and magnitude of Miocene Eustasy derived from the mixed siliciclastic-carbonate stratigraphic record of the northeastern Australian margin. *Earth and Planetary Science Letters*, *304*(3), 455–467. https://doi.org/10.1016/j.epsl.2011.02.013

Kim, J.-H, Romero, O. E., Lohmann, G., Donner, B., Laepple, T., Haam, E., et al. (2012). Pronounced subsurface cooling of North Atlantic waters off Northwest Africa during Dansgaard–Oeschger interstadials. *Earth and Planetary Science Letters*, *339–340*, 95–102. https://doi.org/10.1016/j.epsl.2012.05.018

Kim, J.-H., Schouten, S., Rodrigo-Gámiz, M., Rampen, S., Marino, G., Huguet, C., et al. (2015). Influence of deep-water derived isoprenoid Tetraether lipids on the TEX86H Paleothermometer in the Mediterranean Sea. *Geochimica et Cosmochimica Acta*, *150*, 125–141. https://doi.org/10.1016/j.gca.2014.11.017

Kleijne, A. (1993). Morphology, taxonomy and distribution of extant coccolithophorids (calcareous nannoplankton).

Kürschner, W. M., Kvaček, Z., & Dilcher, D. L. (2008). The impact of Miocene atmospheric carbon dioxide fluctuations on climate and the evolution of terrestrial ecosystems. *Proceedings of the National Academy of Sciences*, *105*(2), 449–453. https://doi.org/10.1073/pnas.0708588105

Lear, C. H., Coxall, H. K., Foster, G. L., Lunt, D. J., Mawbey, E. M., Rosenthal, Y., et al. (2015). Neogene ice volume and ocean temperatures: Insights from infaunal foraminiferal Mg/Ca paleothermometry. *Paleoceanography*, *2006*(11), 1437–1454. https://doi.org/10.1002/2015PA002833

Lear, C. H., Elderfield, H., & Wilson, P. A. (2000). Cenozoic deep-sea temperatures and global ice volumes from Mg/Ca in benthic foraminiferal calcite. *Science*, *287*(5451), 269–272. https://doi.org/10.1126/science.287.5451.269

LeGrande, A. N., & Schmidt, G. A. (2006). Global gridded data set of the oxygen isotopic composition in seawater. *Geophysical Research Letters*, *33*, L12604. https://doi.org/10.1029/2006gl026011

Leutert, T. J., Modestou, S., Bernasconi, S. M., & Meckler, A. N. (2021). Southern ocean bottom-water cooling and ice sheet expansion during the middle Miocene climate transition. *Climate of the Past*, *17*(5), 2255–2271. https://doi.org/10.5194/cp-17-2255-2021

Levy, R., Harwood, D., Florindo, F., Sangiorgi, F., Tripati, R., von Eynatten, H., et al. (2016). Antarctic ice sheet sensitivity to atmospheric CO_2 variations in the early to mid-Miocene. *Proceedings of the National Academy of Sciences of the United States of America*, *113*(13), 3453–3458. https://doi.org/10.1073/pnas.1516030113

Levy, R. H., Meyers, S. R., Naish, T. R., Golledge, N. R., McKay, R. M., Crampton, J. S., et al. (2019). Antarctic ice-sheet sensitivity to obliquity forcing enhanced through ocean connections. *Nature Geoscience*, *12*(2), 132–137. https://doi.org/10.1038/s41561-018-0284-4

Locarnini, M., Mishonov, A., Baranova, O., Boyer, T., Zweng, M., Garcia, H., et al. (2018). *World Ocean atlas 2018, volume 1: Temperature (Vol. 81)*. NOAA Atlas NESDIS.52.

Lynch-Stieglitz, J., Curry, W. B., & Slowey, N. (1999). A geostrophic transport estimate for the Florida Current from the oxygen isotope composition of benthic foraminifera. *Paleoceanography*, *14*(3), 360–373. https://doi.org/10.1029/1999PA900001

M'Boule, D., Chivall, D., Sinke-Schoen, D., Sinninghe Damsté, J. S., Schouten, S., & van der Meer, M. T. J. (2014). Salinity dependent hydrogen isotope fractionation in Alkenones produced by coastal and open ocean haptophyte algae. *Geochimica et Cosmochimica Acta*, *130*, 126–135. https://doi.org/10.1016/j.gca.2014.01.029

Meckler, A. N., Sexton, P. F., Piasecki, A. M., Leutert, T. J., Marquardt, J., Ziegler, M., et al. (2022). Cenozoic evolution of deep ocean temperature from clumped isotope thermometry. *Science*, *377*(6601), 86–90. https://doi.org/10.1126/science.abk0604

Miller, K. G., Browning, J. V., John Schmelz, W., Kopp, R. E., Mountain, G. S., & Wright, J. D. (2020). Cenozoic sea-level and Cryospheric evolution from deep-sea geochemical and continental margin records. *Science Advances*, *6*(20), eaaz1346. https://doi.org/10.1126/sciadv.aaz1346

Miller, K. G., Feigenson, M. D., Wright, J. D., & Clement, B. M. (1991). Miocene isotope reference section, Deep Sea Drilling Project Site 608: An evaluation of isotope and biostratigraphic resolution. *Paleoceanography*, *6*(1), 33–52. https://doi.org/10.1029/90PA01941

Mitsunaga, B. A., Novak, J., Zhao, X., Dillon, J. A., Huang, Y., & Herbert, T. D. (2022). Alkenone δ^2H values – A viable seawater isotope proxy? New core-top δ^2H$_{C37:3}$ and δ^2H$_{C37:2}$ data suggest inter-alkenone and alkenone-water hydrogen isotope fractionation are independent of temperature and salinity. *Geochimica et Cosmochimica Acta*, *339*, 139–156. https://doi.org/10.1016/j.gca.2022.10.024

Modestou, S. E., Leutert, T. J., Fernandez, A., Lear, C. H., & Meckler, A. N. (2020). Warm middle Miocene Indian ocean bottom water temperatures: Comparison of clumped isotope and Mg/Ca-based estimates. *Paleoceanography and Paleoclimatology*, *35*(11), e2020PA003927. https://doi.org/10.1029/2020PA003927

Mudelsee, M., Bickert, T., Lear, C. H., & Lohmann, G. (2014). Cenozoic climate changes: A review based on time series analysis of marine benthic δ^{18}O records. *Reviews of Geophysics*, *52*(3), 333–374. https://doi.org/10.1002/2013RG000440

Müller, P. J., Kirst, G., Ruhland, G., von Storch, I., & Rosell-Melé, A. (1998). Calibration of the alkenone Paleotemperature index U37K′ based on core-tops from the eastern South Atlantic and the global ocean (60°N-60°S). *Geochimica et Cosmochimica Acta*, *62*(10), 1757–1772. https://doi.org/10.1016/S0016-7037(98)00097-0

Pagani, M., Arthur, M. A., & Freeman, K. H. (1999). Miocene evolution of atmospheric carbon dioxide. *Paleoceanography*, *14*(3), 273–292. https://doi.org/10.1029/1999PA900006

Passchier, S., Browne, G., Field, B., Fielding, C. R., Krissek, L. A., Panter, K., et al. (2011). Early and middle Miocene Antarctic glacial history from the sedimentary Facies distribution in the AND-2A drill hole, Ross sea, Antarctica. *Bulletin of the Geological Society of America*, *123*(11–12), 2352–2365. https://doi.org/10.1130/B30334.1

Pearson, P., Ditchfield, P., Singano, J., Harcourt-Brown, K. G., Nicholas, C. J., Olsson, R. K., et al. (2001). Warm tropical sea surface temperatures in the Late Cretaceous and Eocene epochs. *Nature*, *413*(6855), 481–487. https://doi.org/10.1038/35097000

Pearson, P. N., van Dongen, B. E., Nicholas, C. J., Pancost, R. D., Schouten, S., Singano, J. M., et al. (2007). Stable warm tropical climate through the Eocene Epoch. *Geology*, *35*(3), 211–214. https://doi.org/10.1130/G23175A.1

Perch-Nielsen, K. (1985). Cenozoic calcareous Nannofossils. In H. M. Bolli, J. B. Sanders, & K. Perch-Nielsen (Eds.), *Plankton stratigraphy*. Cambridge University Press.

Pierce, E. L., van de Flierdt, T., Williams, T., Hemming, S. R., Cook, C. P., & Passchier, S. (2017). Evidence for a dynamic East Antarctic ice sheet during the mid-Miocene climate transition. *Earth and Planetary Science Letters*, *478*, 1–13. https://doi.org/10.1016/j.epsl.2017.08.011

Prahl, F. G., & Wakeham, S. G. (1987). Calibration of unsaturation patterns in long-chain ketone compositions for palaeotemperature assessment. *Nature*, *330*(6146), 367–369. https://doi.org/10.1038/330367a0

Quaijtaal, W., Donders, T. H., Persico, D., & Louwye, S. (2014). Characterising the middle Miocene mi-events in the Eastern North Atlantic realm: A first high-resolution marine Palynological record from the Porcupine Basin. *Palaeogeography, Palaeoclimatology, Palaeoecology*, *399*, 140–159. https://doi.org/10.1016/j.palaeo.2014.02.017

Quaijtaal, W., Tesseur, S., Donders, T. H., Claeys, P., & Louwye, S. (2018). A revised and improved age model for the middle Miocene part of IODP Site U1318 (Porcupine Basin, offshore southwestern Ireland). *Geological Magazine*, *155*(5), 1105–1116. https://doi.org/10.1017/S0016756816001278

Raddatz, J., Rüggeberg, A., Margreth, S., & Dullo, W. C. (2011). Paleoenvironmental reconstruction of challenger mound initiation in the porcupine seabight, NE Atlantic. *Marine Geology*, *282*(1–2), 79–90. https://doi.org/10.1016/j.margeo.2010.10.019

Rice, A. L., Billett, D. S. M., Thurston, M. H., & Lampitt, R. S. (1991). The institute of oceanographic sciences biology programme in the porcupine seabight: Background and general introduction. *Journal of the Marine Biological Association of the United Kingdom*, *71*(2), 281–310. https://doi.org/10.1017/S0025315400051614

Rohling, E. J. (2007). Progress in paleosalinity: Overview and presentation of a new approach. *Paleoceanography*, *22*(3), 1–9. https://doi.org/10.1029/2007PA001437

Rohling, E. J., Foster, G. L., Gernon, T. M., Grant, K. M., Heslop, D., Hibbert, F. D., et al. (2022). Comparison and synthesis of seasea-level and deep-sea temperature variations over the past 40 million years. *Reviews of Geophysics*, *60*(4), e2022RG000775. https://doi.org/10.1029/2022RG000775

Ryan, W. B. F., Carbotte, S. M., Coplan, J. O., O'Hara, S., Melkonian, A., Arko, R., et al. (2009). Global multi-resolution topography synthesis. *Geochemistry, Geophysics, Geosystems*, *10*(3), Q03014. https://doi.org/10.1029/2008GC002332

Sachs, J. P., Maloney, A. E., & Gregersen, J. (2017). Effect of light on 2H/1H fractionation in lipids from continuous cultures of the diatom Thalassiosira pseudonana. *Geochimica et Cosmochimica Acta*, *209*, 204–215. https://doi.org/10.1016/j.gca.2017.04.008

Sachs, J. P., Maloney, A. E., Gregersen, J., & Paschall, C. (2016). Effect of salinity on 2H/1H fractionation in lipids from continuous cultures of the coccolithophorid Emiliania huxleyi. *Geochimica et Cosmochimica Acta*, *189*, 96–109. https://doi.org/10.1016/j.gca.2016.05.041

Samtleben, C. (1980). Die Evolution der Coccolithophoriden-GattungGephyrocapsa nach Befunden im Atlantik. *Paläontologische Zeitschrift*, *54*(1), 91–127. https://doi.org/10.1007/BF02985885

Sangiorgi, F., Bijl, P. K., Passchier, S., Salzmann, U., Schouten, S., McKay, R., et al. (2018). Southern Ocean warming and Wilkes Land ice sheet retreat during the mid-Miocene. *Nature Communications*, *9*(1), 317. https://doi.org/10.1038/s41467-017-02609-7

Sangiorgi, F., Quaijtaal, W., Donders, T. H., Schouten, S., & Louwye, S. (2021). Middle Miocene Temperature and Productivity Evolution at a Northeast Atlantic Shelf Site (IODP U1318, Porcupine Basin): Global and Regional Changes. C. *Paleoceanography and Paleoclimatology*, *36*(7), e2020PA004059. https://doi.org/10.1029/2020PA004059

Savin, S. M., Douglas, R., & Stehli, F. G. (1975). Tertiary marine paleotemperatures. *GSA Bulletin*, *86*(11), 1499–1510. https://doi.org/10.1130/0016-7606(1975)86<1499:TMP>2.0.CO;2

Schouten, S., Hopmans, E. C., Schefuß, E., & Sinninghe Damsté, J. S. (2002). Distributional variations in marine crenarchaeotal membrane lipids: A new tool for reconstructing ancient sea water temperatures? *Earth and Planetary Science Letters*, *204*(1–2), 265–274. https://doi.org/10.1016/S0012-821X(02)00979-2

Schouten, S., Ossebaar, J., Schreiber, K., Kienhuis, M. V. M., Langer, G., Benthien, A., et al. (2006). The effect of temperature, salinity and growth rate on the stable hydrogen isotopic composition of long chain Alkenones produced by Emiliania huxleyi and Gephyrocapsa oceanica. *Biogeosciences*, *3*(1), 113–119. https://doi.org/10.5194/bg-3-113-2006

Sexton, P. F., & Wilson, P. A. (2009). Preservation of benthic foraminifera and reliability of deep-sea temperature records: Importance of sedimentation rates, lithology, and the need to examine test wall structure. *Paleoceanography*, *24*(2), PA2208. https://doi.org/10.1029/2008PA001650

Shackleton, N. J. (1974). Attainment of isotopic equilibrium between ocean water and the benthonic foraminifera Geuns Uvigerina: Isotopic changes in the ocean during the last glacial. *Colloques Internationaux Du C.N.R.S.*, *219*, 203–210.

Shevenell, A. E., Kennett, J. P., & Lea, D. W. (2004). Middle Miocene Southern Ocean Cooling and Antarctic Cryosphere Expansion. *Science*, *305*(5691), 1766–1770. https://doi.org/10.1126/science.1100061

Shevenell, A. E., Kennett, J. P., & Lea, D. W. (2008). Middle Miocene ice sheet dynamics, deep-sea temperatures, and carbon cycling: A Southern Ocean perspective. *Geochemistry, Geophysics, Geosystems*, *9*(2), Q02006. https://doi.org/10.1029/2007GC001736

Sosdian, S., & Rosenthal, Y. (2009). Deep-Sea Temperature and Ice volume changes across the Pliocene-Pleistocene Climate Transitions. *Science*, *325*(5938), 306–310. https://doi.org/10.1126/science.1169938

Sosdian, S. M., Greenop, R., Hain, M. P., Foster, G. L., Pearson, P. N., & Lear, C. H. (2018). Constraining the evolution of Neogene ocean carbonate chemistry using the boron isotope pH proxy. *Earth and Planetary Science Letters*, *498*, 362–376. https://doi.org/10.1016/j.epsl.2018.06.017

Sosdian, S. M., & Lear, C. H. (2020). Initiation of the Western Pacific Warm Pool at the Middle Miocene Climate Transition? *Paleoceanography and Paleoclimatology*, *35*(12), e2020PA003920. https://doi.org/10.1029/2020PA003920

Srivastava, R., Ramesh, R., Jani, R. A., Anilkumar, N., & Sudhakar, M. (2010). Stable oxygen, hydrogen isotope ratios and salinity variations of the surface Southern Indian Ocean waters. *Current Science*, *99*(10), 1395–1399.

Steinthorsdottir, M., Coxall, H. K., de Boer, A. M., Huber, M., Barbolini, N., Bradshaw, C. D., et al. (2021). The Miocene: The Future of the Past. *Paleoceanography and Paleoclimatology*, *36*(4), e2020PA004037. https://doi.org/10.1029/2020PA004037

Super, J. R., Thomas, E., Pagani, M., Huber, M., O'Brien, C., & Hull, P. M. (2018). North Atlantic temperature and pCO_2 coupling in the early-middle Miocene. *Geology*, *46*(6), 519–522. https://doi.org/10.1130/G40228.1

Taylor, K. W. R., Huber, M., Hollis, C. J., Hernandez-Sanchez, M. T., & Pancost, R. D. (2013). Re-evaluating modern and Palaeogene GDGT distributions: Implications for SST reconstructions. *Global and Planetary Change*, *108*, 158–174. https://doi.org/10.1016/j.gloplacha.2013.06.011

van der Meer, M. T. J., Benthien, A., French, K. L., Epping, E., Zondervan, I., Reichart, G. J., et al. (2015). Large effect of irradiance on hydrogen isotope fractionation of alkenones in Emiliania Huxleyi. *Geochimica et Cosmochimica Acta*, *160*, 16–24. https://doi.org/10.1016/j.gca.2015.03.024

Van Hinsbergen, D. J. J., De Groot, L. V., Van Schaik, S. J., Spakman, W., Bijl, P. K., Sluijs, A., et al. (2015). A paleolatitude calculator for paleoclimate studies. *PLoS One*, *10*(6), e0126946. https://doi.org/10.1371/journal.pone.0126946

Varma, D., Hättig, K., van der Meer, M. T. J., Reichart, G.-J., & Schouten, S. (2023). Constraining water depth influence on organic paleo-temperature proxies using sedimentary archives. *Paleoceanography and Paleoclimatology*, *38*(6), e2022PA004533. https://doi.org/10.1029/2022PA004533

Warny, S., Askin, R. A., Hannah, M. J., Mohr, B. A. R., Raine, J. I., Harwood, D. M., et al. (2009). Palynomorphs from a sediment core reveal a sudden remarkably warm Antarctica during the middle Miocene. *Geology*, *37*(10), 955–958. https://doi.org/10.1130/G30139A.1

Weiss, G. M., Schouten, S., Sinninghe Damsté, J. S., & van der Meer, M. T. J. (2019). Constraining the application of hydrogen isotopic composition of alkenones as a salinity proxy using marine surface sediments. *Geochimica et Cosmochimica Acta*, *250*, 34–48. https://doi.org/10.1016/j.gca.2019.01.038

Weiss, M. G., Pfannerstill, Y. E., Schouten, S., Sinninghe Damsté, S. J., & Van Der Meer, T. J. M. (2017). Effects of alkalinity and salinity at low and high light intensity on hydrogen isotope fractionation of long-chain alkenones produced by Emiliania Huxleyi. *Biogeosciences*, *14*(24), 5693–5704. https://doi.org/10.5194/bg-14-5693-2017

Westerhold, T., Marwan, N., Drury, A. J., Liebrand, D., Agnini, C., Anagnostou, E., et al. (2020). An astronomically dated record of Earth's climate and its predictability over the last 66 million years. *Science*, *369*(6509), 1383–1388. https://doi.org/10.1126/SCIENCE.ABA6853

Wienberg, C., Titschack, J., Frank, N., Pol-Holz, R. D., Fietzke, J., Eisele, M., et al. (2020). Deglacial upslope shift of NE Atlantic intermediate waters controlled slope erosion and cold-water coral mound formation (Porcupine Seabight, Irish margin). *Quaternary Science Reviews*, *237*, 106310. https://doi.org/10.1016/j.quascirev.2020.106310

Wolfshorndl, M., Danford, R., & Sachs, J. P. (2019). 2H/1H fractionation in microalgal lipids from the North Pacific Ocean: Growth rate and irradiance effects. *Geochimica et Cosmochimica Acta*, *246*, 317–338. https://doi.org/10.1016/j.gca.2018.11.027

Wolhowe, M. D., Prahl, F. G., Langer, G., Oviedo, A. M., & Ziveri, P. (2015). Alkenone δD as an ecological indicator: A culture and field study of physiologically-controlled chemical and hydrogen-isotopic variation in C_{37} alkenones. *Geochimica et Cosmochimica Acta*, *162*, 166–182. https://doi.org/10.1016/j.gca.2015.04.034

Zachos, J. C., Dickens, G. R., & Zeebe, R. E. (2008). An early Cenozoic perspective on greenhouse warming and carbon-cycle dynamics. *Nature*, *451*(7176), 279–283. https://doi.org/10.1038/nature06588

Zhang, Y. G., Pagani, M., Liu, Z., Bohaty, S. M., & Deconto, R. (2013). A 40-million-year history of atmospheric CO_2. *Philosophical Transactions of the Royal Society A: Mathematical, Physical & Engineering Sciences*, *371*(2001), 20130096. https://doi.org/10.1098/rsta.2013.0096

Zhang, Z., & Sachs, J. P. (2007). Hydrogen isotope fractionation in freshwater algae: I. Variations among lipids and species. *Organic Geochemistry*, *38*(4), 582–608. https://doi.org/10.1016/j.orggeochem.2006.12.004

Zhang, Z., Sachs, J. P., & Marchetti, A. (2009). Hydrogen isotope fractionation in freshwater and marine algae: II. Temperature and nitrogen limited growth rate effects. *Organic Geochemistry*, *40*(3), 428–439. https://doi.org/10.1016/j.orggeochem.2008.11.002

Zweng, M. M., Reagan, J. R., Seidov, D., Boyer, T. P., Locarnini, R. A., Garcia, H. E., et al. (2018). World Ocean Atlas 2018, Volume 2: Salinity. A. Mishonov Technical Ed.; NOAA Atlas NESDIS 82, 50pp. In *World Ocean atlas 2018* (Vol. 2).